Int. J. Heat Mass Transfer. Vol. 28, No. 7, pp. 1307–1316, 1985
Printed in Great Britain

0017-9310/85 $3.00 + 0.00

A bubble growth model for nucleate boiling in thin, falling, superheated, laminar, water films

M. CERZA
Naval Underwater Systems Center, New London Laboratory, Code 3322, New London, CT 06320, U.S.A.

and

V. SERNAS
Rutgers University, Department of Mechanical and Aerospace Engineering, PO Box 909, Piscataway, NJ 08854, U.S.A.

(*Received* 5 *July* 1984 *and in final form* 2 *January* 1985)

Abstract—An analytical and experimental investigation into the mechanism for bubble growth in a thin, falling, superheated, laminar, water film has been conducted. The majority of bubble growth is seen to be caused by transient heat conduction through the bubble base while the bubble is swept away by the falling film. The observed bubble heat rates are significantly larger than that which would occur from film surface evaporization alone. This indicates that the bubble base lies imbedded in the ambient film thickness. The proposed model is applicable to cases where the wall heat flux results in negligible bubble base mass transfer.

INTRODUCTION

NUCLEATE boiling in pools is distinctly different from nucleate boiling in thin, falling liquid films. In nucleate pool boiling, bubbles grow from cavity sites along the heated wall [1]. Bubble growth is generally confined to the thickness of the superheated thermal layer next to the heated wall [2, 3]. A pool bubble grows both due to transient conduction from the thermal layer located above the bubble cap and due to evaporation from the superheated microlayer at the bubble's base (Fig. 1). Once the pool bubble departs from its site, it rises through a pool of saturated liquid. Very little additional growth occurs in this phase of the bubble's life.

Bubbles in falling liquid films, on the other hand, have been observed by high speed photography to continue to grow rapidly after they have been detached from their nucleating sites and are swept downstream by the falling film [4–8]. These bubbles were seen to detach from their sites at diameters larger than the ambient film thickness. They also grew to diameters that were an order of magnitude larger than the film thickness (Fig. 2). The growth rates of these bubbles have been observed to be several times the growth rate which would result from film surface evaporation alone. No mathematical attempt has yet been made to model the mechanism responsible for this heat transfer phenomenon. Furthermore, the expressions for the growth rate of bubbles in nucleate pool boiling [9–12] underestimate the growth rate of bubbles in a falling superheated liquid film.

A vapor bubble in a falling superheated liquid film has many stages of growth: a waiting stage, an unbinding stage, and a freestream growth stage. The waiting stage is the time between the departure of a bubble from a given site and the appearance of the next bubble. In nucleate pool boiling, this stage was found to vary approximately between 4 and 25 ms, depending on boiling conditions [2, 3]. There is no substantial growth during this period. The unbinding stage is the time between the appearance of a bubble at its site and

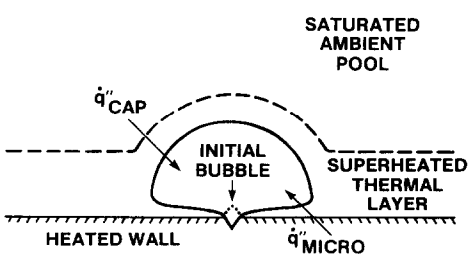

FIG. 1. Pool boiling bubble.

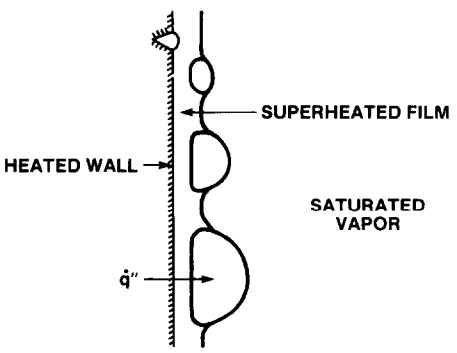

FIG. 2. Thin, falling film boiling.

NOMENCLATURE

A_b	bubble base area
g	acceleration of gravity
h_{fg}	latent heat of vaporization
k	liquid film thermal conductivity
$\dot{q}_b$	instantaneous bubble heat rate
$\dot{q}_{chord}$	bubble base chord heat rate
R	theoretical bubble radius
Re	film Reynolds number, $4\Gamma/\mu$
R_{eq}	equivalent bubble radius from experiment
R_0	initial bubble radius
t	time
T	temperature
T_s	saturation temperature
T_w	heated wall temperature
U_b	bubble center velocity
v	velocity of fluid beneath bubble base
V_0	velocity of fluid at bubble base
V_{SLIP}	$U_b - V_0$
V_{TOT}	total bubble volume
x, y, z, ϕ	coordinates.

Greek symbols

α	fluid thermal diffusivity
Γ	mass flow rate per unit tube periphery
δ_b	thickness beneath bubble base
δ_f	ambient film thickness
λ	eigenvalue
ρ_g	density of gas within bubble
θ	$T - T_s$
μ	dynamic viscosity
ν	kinematic viscosity.

its departure from that site. During this period in nucleate pool boiling, the bubble is growing rapidly and is trying to detach itself from the heated wall. The majority of a pool bubble's growth occurs during this stage [11]. In the boiling of a thin falling film, the amount of growth during the unbinding stage is small compared to the freestream growth stage because the freestream growth period is significantly longer than the unbinding stage [8]. The period of freestream growth is the life of the bubble after it departs from its site until it vents. This freestream growth stage is, therefore, the major growth period for a bubble in a falling superheated liquid film. During this stage, bubble growth is entirely dominated by transient heat conduction.

The purpose of this paper is to analytically model, and experimentally substantiate, the bubble growth of a single, isolated bubble as it is swept downstream by a thin, superheated, thermally developed, laminar, liquid film. Motion picture photography is employed to measure the approximate bubble volumetric rate of change from which the experimental radial growth history for the isolated bubble can be obtained. An analytical model for the radial growth rate of an isolated bubble is then presented and compared with that of the experimental data. Finally, parametric effects of significant model variables are discussed.

EXPERIMENTAL APPROACH AND PROCEDURE

The experimental test section designed for this study is shown in Fig. 3. It consisted of a 85–15 Red Brass tube, 6.03 cm O.D., 93 cm long and electrically heated from the inside for the first 25 cm of length. A 6.03-cm hemispherical brass cap was soldered to the top of this tube. On the inner side of the heated brass tube were 16 copper–constantan thermocouples imbedded into the tube wall at four circumferential locations and four axial locations. The brass tube and cap were enclosed inside a 15.2-cm O.D. Pyrex pipe with blind aluminum flanges fixed at the top and bottom. The water flow was introduced through a 1.27-cm copper tube which protruded through the center of the top flange and which was centered approx. 1 cm above the center of the brass cap. The water was always close to saturation temperature and it spread itself fairly uniformly over the cap and then flowed down the side of the brass tube. Flow uniformity was checked by visual alignment of the water jet and by wall temperature measurement uniformity around the tube circumference. The water formed a pool at the bottom of the Pyrex pipe where two 1-kW immersion heaters maintained the pool and test chamber environment at saturated conditions. An outlet through the bottom flange led the water to first a recirculation pump, then through a flowmeter to a preheater where sufficient heat was added to bring the

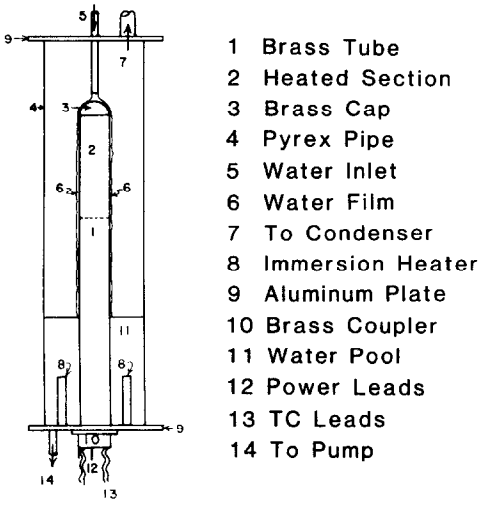

FIG. 3. Experimental test chamber.

temperature of the water back up to saturation temperature. A free surface existed within the preheater so that the vapor formed by an electric immersion heater separated from the liquid. The vapor from the preheater and the test chamber was fed to a condenser where it is was condensed and introduced back into the circulation loop upstream of the pump. The flow in the tube supplying saturated water from the preheater to the test chamber was produced by the hydrostatic head difference between the free surface in the preheater and the brass cap in the test chamber. The pressure in the test chamber was maintained by coupling the test chamber and condenser to a drum that could be regulated by an independent pressure control system.

The test chamber required approximately 1.5 h of operation to reach saturation conditions under atmospheric pressure. An additional 0.5–1 h was required in order to completely outgas the air from the test environment.

A Hycam 16-mm high speed movie camera was utilized with backdrop lighting to produce 16-mm motion picture photographic results. The bubbles appeared on the movie film as silhouette outlines on a bright backdrop. The brass tube appeared dark. Dimensional data of the bubbles was obtained by using the diameter of the blacked out tube as the length scale.

It was experimentally determined that for film flow rates below a Reynolds number of approx. 3000, the flowfield on the cylindrical brass tube would remain laminar for approx. 3–8 cm from the top. An entry length analysis was also made to assure a fully developed flowfield by the time the flow had reached the brass cap–tube seam. It was experimentally possible, by adjusting the heat flux, to have only one site nucleate in the laminar portion of the film. Moreover, it was possible to reduce the nucleating frequency of this site so that vapor bubbles would be produced at a low rate. The production of bubbles at a low frequency ensured that the falling film thermal profile would re-establish itself in the time between the departure of succeeding bubbles. Each departing bubble could then be considered as 'isolated'. Figure 4 shows a head on view of a series of bubbles coming from a single nucleation site in a laminar region of the tube. However, this figure does not depict the bubbles at a 'low' frequency.

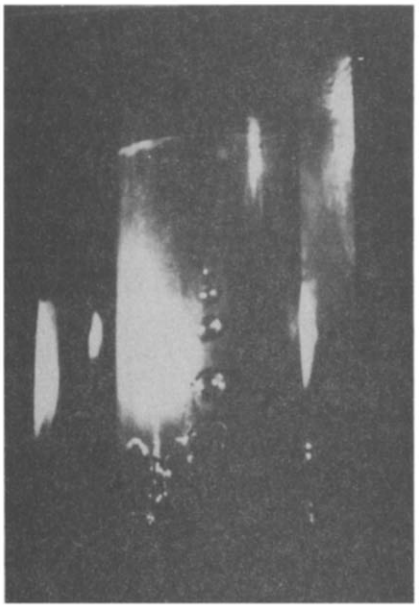

FIG. 4. Bubble site in a laminar regime.

EXPERIMENTAL ANALYSIS OF ISOLATED BUBBLES

A site, nucleating in the laminar flow region of the tube, was captured on film with the Hycam movie camera set at 750 frames s^{-1}. The site was approx. 6 cm from the seam and believed to be in the thermally developed regime, as analyzed by the thermal entry length solution for the laminar flow field [8]. The experimental conditions were: film Reynolds number, 2070; wall heat flux, 30.1 kW m^{-2} and the ambient and inlet saturation temperatures were 99.9°C. Thermocouple measurements indicated a wall superheat of approx. 9°C at the location of the site and at locations on the tube below the site. Several bubbles in the movie appeared to be isolated because they were preceded by a sufficiently long waiting period.

Measurements taken from the movie film showed that the isolated bubbles accelerated to a terminal velocity within 2 or 3 frames from nucleation. One frame represented 1.379 ms of elapsed time. The bubbles were within the camera field of view for approx. 35 frames (48 ms). After the second or third frame, however, slight velocity fluctuations did exist but could not be distinguished as fluctuations caused by film flow phenomena, i.e. waviness, or that caused by bubble dimensional measurement error. In order to simplify the analysis, the bubble drift velocity was taken as constant, averaged from the data on the second to 35th frame. This velocity was determined to be approx. 830 mm s^{-1} for all the bubbles investigated. For the film Reynolds number of 2070, the ambient film thickness was estimated as 0.24 mm based on Nusselt's theory for a laminar film. This estimate yielded film surface and film average velocities of 960 and 640 mm s^{-1}, respectively.

Figure 5 shows the bubble dimensions measured from the movie frames. These dimensions were utilized to approximate bubble volumes in order to calculate bubble growth rates via the change in estimated bubble volume over a specified number of frames. The instantaneous bubble volume was estimated as

$$V_{TOT} \approx V_{CAP} + V_{CYL} + V_{IMB}, \quad (1)$$

where

$$V_{CAP} = \frac{\pi}{6}(B-A)\left\{\frac{3C^2}{4} + (B-A)^2\right\}$$

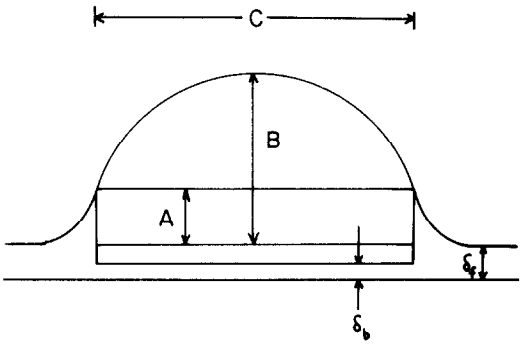

FIG. 5. Bubble dimensional data model.

represents the volume of the truncated sphere above the bubble junction ring (which is the ring that separates the bubble cap from the meniscus),

$$V_{CYL} = \frac{\pi}{4} C^2 A$$

represents the cylindrical volume from the bubble junction ring to the film free surface and

$$V_{IMB} = \frac{\pi C^2}{4} (\delta_f - \delta_b)$$

represents the cylindrical volume beneath the film free surface to the bubble base. Note that the error introduced by using cylindrical volumes is quite small since the bubbles are much larger than the film thickness (Fig. 5 is not to scale). For a bubble much larger than the thickness of its underlying fluid and in close proximity to a wall, the central region of its base is assumed to be almost flat.

In equation (1), a value for the film thickness beneath the bubble base, δ_b, is needed. This quantity could not be obtained in the present investigation without employing measurement techniques that would disturb the flowfield. Comment on the thickness δ_b will be reserved for the next section. As far as the experimental data and equation (1) are concerned, however, the variation of δ_b within the ambient film thickness, δ_f, has a negligible effect on the total bubble volume since the bubble caps were much larger than the ambient film thickness.

The approximate, instantaneous bubble heat rate can be obtained from its volumetric rate of change,

$$\dot{q}_b = \rho_g h_{fg} \frac{d(V_{TOT})}{dt} \approx \rho_g h_{fg} \frac{\Delta V_{TOT}}{\Delta t}. \quad (2)$$

The mathematical model for bubble growth in the next section employs a hemispherical bubble. The heat rate obtained from equation (2) should then be set equal to the heat rate for a hemispherical volume change. This defines an equivalent radius as that radius whose associated hemispherical volume equals the volume as calculated by equation (1). Hence,

$$\dot{q}_b = \rho_g h_{fg} 2\pi R_{eq}^2 \frac{dR_{eq}}{dt}. \quad (3)$$

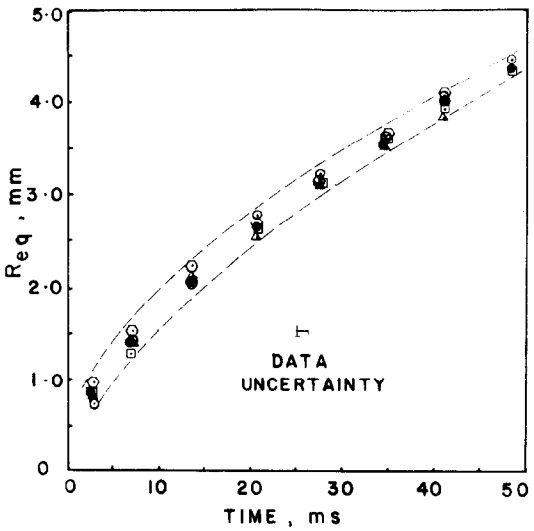

FIG. 6. Radial history of isolated bubbles taken at $Re = 2070$, $q''_w = 30.1$ kW m^{-2} and $T_s = 99.9$°C.

The experimental data has been reduced to equivalent radii and is represented in a plot of R_{eq} vs time in Fig. 6. The dashed lines on the figure represent the envelopes of the data. There are three primary reasons for the scattering of the experimental data. The first is the probability that no two bubbles have the same initial diameter when they leave their site. There may be slight variations in initial size brought about by changes in site conditions. The second reason is the uncertainty in the time of initial bubble appearance. Data was taken from the point where a bubble was first observed on the movie film. Since the camera shoots in discrete frame intervals, the first appearance of a bubble can be at any time within the time associated with 1 frame (1.379 ms). A curve representing a specific bubble could therefore be shifted 1.379 ms to the left on Fig. 6. The third reason for data scatter is error in the actual bubble dimensional measurement. The accuracy in bubble dimensional data measurement from the movie screen was ± 0.03 mm. With the consideration of these three uncertainties, the actual experimental data is quite reasonable. Other causes for measurement error might be related to slight shifts in frame location on the screen as the frames were advanced.

ANALYTICAL MODEL FOR GROWTH OF AN ISOLATED BUBBLE

Vapor bubbles falling in a thin, liquid film are believed to lie imbedded in the liquid film. This idea was further substantiated by an experiment of Sernas and Stanzione [13] in which soap bubbles on a flowing soapy water film were shown to be imbedded in the film. An order-of-magnitude estimate has shown that the majority of bubble growth is caused by the heat flux through the bubble base. Growth via heat conduction through the submerged bubble side wall for the present data was negligible. This was later confirmed by an

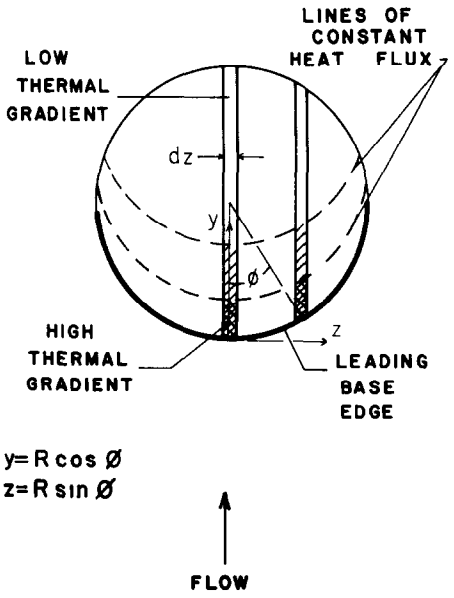

FIG. 7. Integration scheme for bubble base heat flux.

alternate model which included the bubble side wall area (not presented here). Heat transfer through the submerged bubble side wall is negligible because the side wall area is much smaller than the bubble base area and the side wall sees an average lower degree of superheat than the bubble base. The proposed heat transfer model, therefore, only attributes bubble growth via transient heat conduction through the bubble base during the freestream growth stage. The presented model will be applicable for cases of wall heat flux which result in small base mass transfer.

Figure 7 shows the scheme employed for the calculation of the heat flux through the bubble base. An order of magnitude estimate showed that heat conduction can be neglected in the y and z directions. Furthermore, convection was shown to be important only in the y direction. The bubble base can therefore be broken up into strips of chord length $2R\cos\phi$ in the y direction. Each chord is independent of the thermal effects of adjacent chords. The leading semicircular base edge, at any given instant in time, represents the initial encounter of the bubble base with superheated liquid. For each chord, the thermal gradient at the bubble base decays in the direction toward the rear of the base. At any instant in time, lines of constant heat flux at the bubble base can be constructed by drawing arcs of the same radius as the instantaneous radius of the bubble base, at a distance y from the origin.

At any given instant in time, the bubble growth rate can be obtained from the total heat rate at its base, i.e.

$$\dot{q}_b = \rho_g h_{fg} 2\pi R^2 \frac{dR}{dt} = \int_{A_b} k\left(\frac{\partial T}{\partial x}\right)_{x=0} dA_b. \quad (4)$$

At the base, the heat rate per chord can be expressed as

$$\dot{q}_{CHORD} = \int_0^{Y=2R\cos\phi} k\left(\frac{\partial T}{\partial x}\right)_{x=0} dy. \quad (5)$$

Thus, the total instantaneous energy rate from the bubble base is

$$\dot{q}_b = 2\int_0^R \int_0^Y k\left(\frac{\partial T}{\partial x}\right)_{x=0} dy\,dz$$
$$= 2\int_0^{\pi/2} \left[\int_0^Y k\left(\frac{\partial T}{\partial x}\right)_{x=0} dy\right] R\cos\phi\, d\phi. \quad (6)$$

Since the adjacent chords are effectively isolated from each other, the thermal gradient in equation (6) can be obtained from a two-dimensional thermal profile of the laminar liquid film beneath the bubble base. The assumptions are:

(1) mass transfer via base evaporization is small;
(2) the film thickness under the bubble base is constant at δ_b;
(3) the velocity profile under the bubble base is parabolic (fully developed) with the bubble base acting as a no-shear boundary;
(4) the bubble translational velocity is much greater than its radial growth velocity (experimentally verified);
(5) the wall temperature under the bubble is constant due to the shortness in time of the event and the large thermal capacity of the brass heater tube (the tube wall was thick);
(6) the tube wall radius of curvature is much larger than the film thickness (Cartesian coordinates);
(7) conduction is only important in the cross-film, x, direction;
(8) the growing bubble is hemispherical;
(9) the liquid is homogeneous, isotropic and incompressible; and
(10) the density of the vapor is small compared to the liquid density.

With the preceding assumptions, the energy equation for the liquid film underneath a bubble base chord reduces to

$$v(x)\frac{\partial T}{\partial y} = \alpha \frac{\partial^2 T}{\partial x^2}. \quad (7)$$

The origin for a chord is placed at the leading semicircular edge of the bubble base. With respect to a reference frame fixed in space, the problem at hand is one of a moving origin. The problem can be transposed and approximated to one of a fixed origin by choosing a reference frame that moves downstream at the velocity of the center of the bubble, U_b. In this reference frame the bubble center is now stopped and the origin is still at the leading semicircular edge of the bubble base. The walls of the bubble move slightly with respect to the stopped bubble center, but as noted in assumption 4, this radial growth velocity is small compared to the bubble translational velocity. Therefore, the overall effect that the bubble radial growth velocity has on the moving coordinate system of the energy equation is assumed to be negligible.

For the coordinate system shown in Fig. 8, the fluid

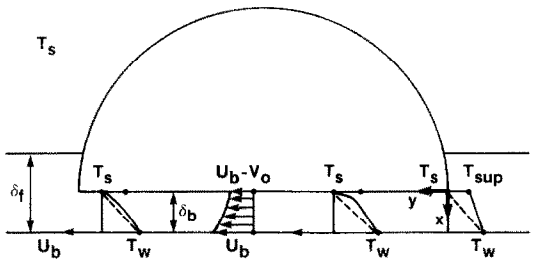

FIG. 8. Schematic of the thermal profiles under the bubble centerline base chord (also shown is the coordinate system and velocity transformation).

velocity profile beneath the bubble base is

$$v(x) = V_0\left(\frac{x}{\delta_b}\right)^2 + V_{SLIP}, \tag{8}$$

where

$$V_0 = \frac{g\delta_b^2}{2\nu}$$

and

$$V_{SLIP} = U_b - V_0.$$

This results in the following differential equation for equation (7),

$$P[\bar{x}^2 + D]\frac{\partial\theta}{\partial y} = \frac{\partial^2\theta}{\partial\bar{x}^2}, \tag{9}$$

where

$$P = \frac{V_0\delta_b^2}{\alpha},$$

$$D = V_{SLIP}/V_0$$

and the following changes in variables have been employed

$$\theta = T - T_s$$

$$\bar{x} = x/\delta_b.$$

The following boundary conditions are imposed on equation (9):

$$\text{at} \quad \bar{x} = 0, \quad \theta = 0; \quad \text{for} \quad y > 0, \tag{10a}$$

$$\text{at} \quad \bar{x} = 1, \quad \theta = \theta_w; \quad \text{for} \quad y > 0 \tag{10b}$$

and

$$\text{at} \quad y = 0, \quad \theta = \theta_{sup} + (\theta_w - \theta_{sup})\bar{x}, \tag{10c}$$

where

$$\theta_{sup} = \theta_w - \left(\frac{\delta_b}{\delta_f}\right)\theta_w.$$

A schematic representation of the temperature profiles under a bubble base chord are also shown in Fig. 8. This figure is consistent with the above boundary conditions and can be thought of as being a slice through a typical chord that has been shown in Fig. 7.

The solution to equation (9) subject to equation (10) is very tedious and contains many mathematical steps. It is similar to a series of problems first encountered by Graetz [14] and later investigated by many others [8, 15–17]. The solution is

$$\theta(\bar{x}, y) = \theta_w\bar{x} + \sum_{k=0}^{\infty} H_k Cz_0(\lambda_k, \bar{x}) \exp\left(\frac{-\lambda_k^2 y}{P}\right), \tag{11}$$

where

$$Cz_0 = \text{odd parabolic cylinder function},$$

$$= \bar{x} + \sum_{n=2}^{\infty} b_{2n-1}\bar{x}^{2n-1};$$

$$b_{2n-1} = \frac{-\lambda_k^2(Db_{2n-3} + b_{2n-5})}{(2n-1)(2n-2)},$$

if m in b_m is <0, then $b_m = 0$, and $b_1 = 1$;

$$H_k = \text{constants} = \frac{2\theta_{sup}}{\lambda_k\left[\dfrac{dCz_0}{d\lambda}\dfrac{dCz_0}{d\bar{x}}\right]_{\bar{x}=1,\,\lambda=\lambda_k}},$$

and λ_k = eigenvalues which can be found from solution of the following equation,

$$\sum_{n=2}^{\infty} b_{2n-1} = -1. \tag{12}$$

The first four terms of the odd parabolic cylinder function, Cz_0, are

$$\bar{x} - \frac{\lambda_k^2 D}{6}\bar{x}^3 + \frac{\lambda_k^2}{20}\left\{\frac{\lambda_k^2 D^2}{6} - 1\right\}\bar{x}^5 - \frac{\lambda_k^4}{42}\left\{\frac{\lambda_k^2 D^3}{120} - \frac{13}{60}D\right\}\bar{x}^7 + \cdots.$$

Equation (11) represents the temperature distribution underneath a bubble base chord at any location, y, and depth, x. In this solution, the parameter $D = V_{SLIP}/V_0$ is a major unknown. D is a measure of the relative slip between the bubble center velocity, U_b, and the velocity of the fluid at the bubble's base, V_0. If the value of this slip parameter is known, then the eigenvalues [equation (12)] can be determined and equation (11) can be solved. The bubble center velocity can be measured by experiment. The thickness below the bubble base, δ_b, could not be measured. This thickness determines the velocity V_0 and the magnitude of the initial superheat encountered at the bubble base leading edge. If δ_b is large, the slip velocity and the initial superheat encountered are both small. This would result in low bubble growth rates. If δ_b is small, the converse applies and larger growth rates would result. An exact determination of the thickness δ_b is difficult and beyond the scope of this investigation. Since other pertinent variables can be accurately measured from experiment, i.e. U_b and θ_w, representative values of δ_b will be chosen to see whether or not theory can be made to correspond with experimental data.

From equation (11) the thermal gradient for a bubble

base chord can be expressed as

$$\left(\frac{\partial T}{\partial x}\right)_{x=0} = \frac{1}{\delta_b}\left(\frac{\partial \theta}{\partial \bar{x}}\right)_{\bar{x}=0} = \frac{1}{\delta_b}\left\{\theta_w + 2\theta_{sup}\sum_{k=0}^{\infty} B_k \exp\left(\frac{-\lambda_k^2 y}{P}\right)\right\}, \quad (13)$$

where

$$B_k = \left\{\lambda_k\left[\frac{dCz_0}{d\lambda}\,\frac{dCz_0}{d\bar{x}}\right]\right\}^{-1}_{\bar{x}=1,\,\lambda=\lambda_k}.$$

The substitution of equation (13) into equation (5) and subsequent integration yields the following heat rate per chord

$$\dot{q}_{CHORD} = \frac{k}{\delta_b}\left\{2\theta_w R\cos\phi + 2P\theta_{sup}\left[\sum_{k=0}^{\infty}\left(\frac{B_k}{\lambda_k^2}\right) - \sum_{k=0}^{\infty}\left(\frac{B_k}{\lambda_k^2}\right)\exp\left(\frac{-\lambda_k^2 2R\cos\phi}{P}\right)\right]\right\} \quad (14)$$

where the substitution $Y = 2R\cos\phi$ was used.

Substitution of equation (14) into equation (6) yields

$$\dot{q}_b = \frac{2Rk}{\delta_b}\int_0^{\pi/2}\left\{2\theta_w R\cos\phi + 2P\theta_{sup}\left[\sum_{k=0}^{\infty}\left(\frac{B_k}{\lambda_k^2}\right) - \sum_{k=0}^{\infty}\left(\frac{B_k}{\lambda_k^2}\right)\exp\left(\frac{-\lambda_k^2 2R\cos\phi}{P}\right)\right]\right\}\cos\phi\,d\phi. \quad (15)$$

The integration of equation (15) yields

$$\dot{q}_b = \frac{k}{\delta_b}\left\{\pi R^2\theta_w + 4RP\theta_{sup}\left[\sum_{k=0}^{\infty}\left(\frac{B_k}{\lambda_k^2}\right) - \sum_{k=0}^{\infty}\left(\frac{B_k}{\lambda_k^2}\right)\times\int_0^{\pi/2}\exp\left(\frac{-\lambda_k^2 2R\cos\phi}{P}\right)\cos\phi\,d\phi\right]\right\}. \quad (16)$$

The radial growth rate can be obtained by equating equations (16) and (4). The result is

$$\frac{dR}{dt} = \frac{k}{\delta_b\rho_g h_{fg}}\left\{\frac{\theta_w}{2} + \frac{2P\theta_{sup}}{\pi R}\left[\sum_{k=0}^{\infty}\left(\frac{B_k}{\lambda_k^2}\right) - \sum_{k=0}^{\infty}\left(\frac{B_k}{\lambda_k^2}\right)\times\int_0^{\pi/2}\exp\left(\frac{-\lambda_k^2 2R\cos\phi}{P}\right)\cos\phi\,d\phi\right]\right\}. \quad (17)$$

Equation (17) can be evaluated via a fourth order Runge–Kutta routine once the parameters U_b and θ_w are experimentally measured, and δ_b is assumed. An initial value for the bubble radius, R_0, is then needed. This can be obtained from the experimental data.

COMPARISON OF MODEL AND EXPERIMENT

The presented analytical model describes the freestream growth period of a bubble while the bubble cap is outside the liquid film. The experimental bubbles, however, incorporated an unbinding period plus a freestream growth period. This posed the problem of how to designate the beginning of the freestream growth period for the experimental bubbles, since during the unbinding period the bubble cap lies within the thin liquid film. A bubble shown on the second frame, however, has actually traversed approx. 1.5 diameters from the location of its nucleating site. The freestream bubble growth model may then be applicable from frame No. 2. An initial bubble radius, R_0, can also be obtained from this frame. Figures 9–12 reflect time zero as starting from the second frame.

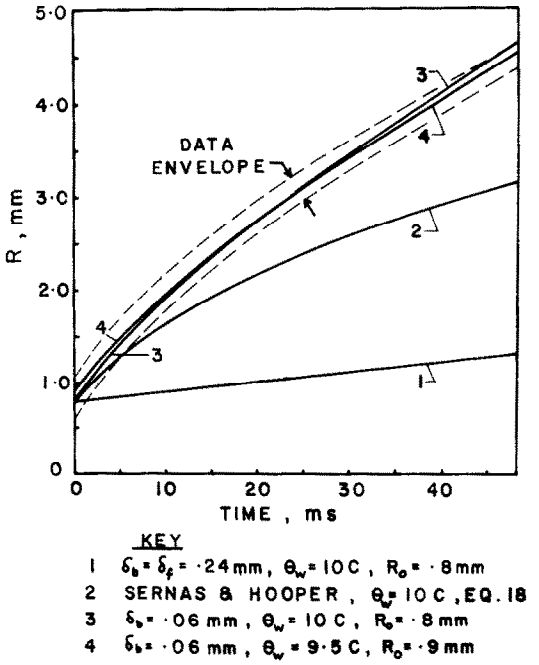

FIG. 9. Comparison of experimental data with various theories.

Curves 3 and 4 of Fig. 9 represent the calculated theoretical bubble radial history from the solution of equation (17). The variables incorporated with curve 3

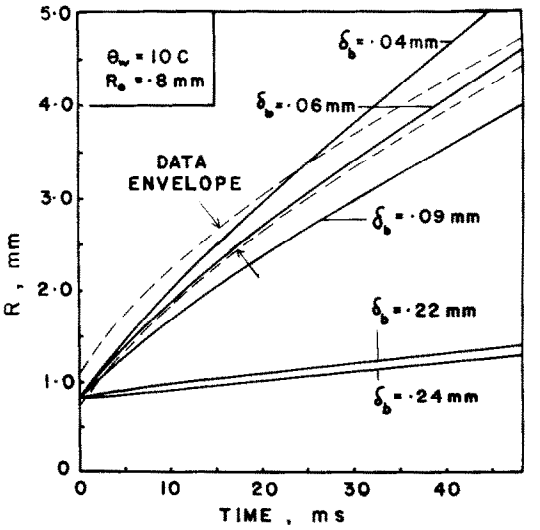

FIG. 10. The effect of the thickness beneath the bubble base on the bubble growth model, equation (17).

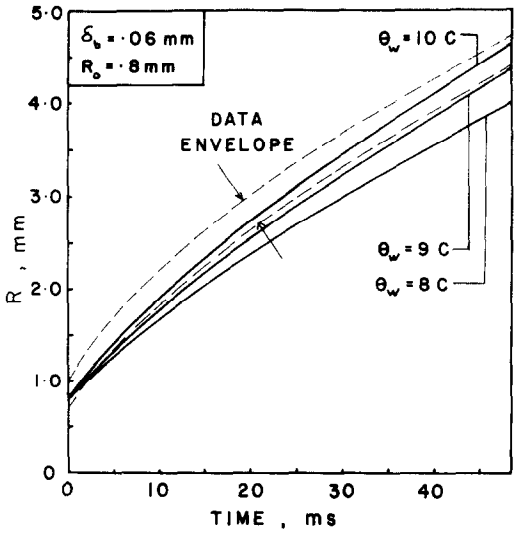

FIG. 11. The effect of wall superheat on the bubble growth model, equation (17).

were: $\delta_f = 0.24$ mm, $\delta_b = 0.06$ mm, $\theta_w = 10°C$ and $R_0 = 0.8$ mm. The variables associated with curve 4 were: $\delta_f = 0.24$ mm, $\delta_b = 0.06$ mm, $\theta_w = 9.5°C$ and $R_0 = 0.9$ mm. As can be seen, both curves give excellent agreement with the envelope of experimental data. The envelope was shifted to the left to take into account the discrepancy in time zero between actual data and model. The reason for showing two curves that correspond well with the experimental data is to reflect the latitude in the uncertainty of the measured data, since the measurement of experimental parameters such as wall superheat and initial bubble radius may be slightly in error. Curve 2 represents a typical pool boiling model, Sernas and Hooper [11], which follows the relationship

$$R = m(t-t')^{1/2}, \tag{18}$$

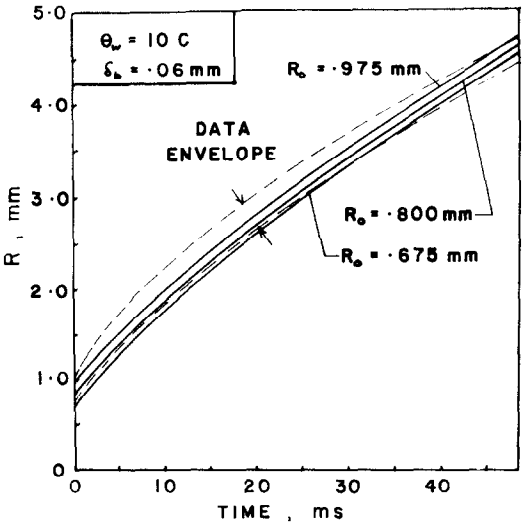

FIG. 12. The effect of the initial bubble radius on the bubble growth model, equation (17).

where

$$m = \frac{2k\theta_w}{\sqrt{\pi\alpha\rho_g h_{fg}}}$$

and t' = the time shift required to make the origin of the experimental data coincide with the origin of the pool model.

Equation (18) reflects evaporation into the bubble from the 'microlayer' under the pool bubble's base only. The wall superheat used in curve 2 was 10°C, and the resulting R_0 is 0.8 mm. It can be seen from Fig. 9 that the pool boiling model underestimates the data. The primary reason for this is in the speed that the pool bubble's base leading edge has as it moves through superheated liquid. The front of a pool bubble can only move through superheated liquid at a velocity equal to its radial growth velocity. This was calculated to be in the vicinity of 90 mm s^{-1} near the start of bubble growth and 35 mm s^{-1} at later stages of bubble life. In the thin film flow model, this leading edge velocity is approx. V_{SLIP}, which for the current data is equal to 770 mm s^{-1}. Thus it can be seen that the bubble in a falling liquid film moves through the superheated liquid an order of magnitude faster than the pool bubble for the current parameters.

Curve 1 of Fig. 9 represents the model of a bubble which sits on the free surface ($\delta_b = \delta_f = 0.24$ mm, $\theta_w = 10°C$ and $R_0 = 0.8$ mm). The base of a bubble of this type (if physically possible) is subjected to the heat rate of surface evaporation only. At 48 ms, the difference in R between curves 4 and 1 is 360% and the associated bubble base heat fluxes for the same curves are 172 and 28 kW m^{-2}, respectively, a difference of over 600%. A real bubble, which is being swept downstream by a thin liquid film, must have its base deeply imbedded in the moving film. This result agrees with that reported by Mesler [18] for bubbles growing in a superheated stationary liquid film.

PARAMETRIC EFFECTS OF MODEL VARIABLES

Curve 4 of Fig. 9 was selected to show the effects of the parameters δ_b, θ_w and R_0 on the thin falling film bubble growth model. On all subsequent figures, the variations in the above selected variables reflect the range of measurement uncertainty associated with that variable, with the exception of δ_b which could not be experimentally measured. Figure 10 shows the effect of the film thickness underneath the bubble base on the radial history for $\theta_w = 10°C$ and $R_0 = 0.8$ mm. The curve for $\delta_b = \delta_f = 0.24$ mm represents the case of a bubble sitting on the ambient film surface. The heat flux through this bubble is equal only to that of surface evaporation and is much too small to justify the observed growth rates. The thickness, $\delta_b = 0.22$ mm, represents the case of 'no slip' between the velocity of the bubble and the fluid which comprises its base, i.e. the bubble base velocity is equal to the bubble center

velocity, 830 mm s^{-1}. This bubble is not sitting deep enough in the underlying liquid film for its calculated growth rate is too small. Thus, one is led to the conclusion that the bubble must lie deeper in the liquid film for the present experimental conditions. A bubble which lies deeper in the film than the previous 'no slip' case will have a slip velocity, if the previously assumed velocity profile (assumption 3) is appropriate. The thicknesses for $\delta_b = 0.09$, 0.06 and 0.04 mm were arbitrarily assumed, and their growth curves plotted on Fig. 10. The last thickness shows too large a growth rate, while the first one too small a growth rate. The case for $\delta_b = 0.06$ mm fits the experimental data very well.

Figure 11 depicts the effect of wall superheat on bubble radius history for $\delta_b = 0.06$ mm and $R_0 = 0.8$ mm. Since the actual measurement of wall superheat was approx. 9°C, a reasonable uncertainty of ± 1°C was used in the generation of the curves. The curves show reasonable agreement between 9 and 10°C. Beyond 10°C, the slope appears too steep when compared to the slope of the 'trend' of the data envelope. Below 8°C, the slope is too shallow.

Figure 12 displays the effect of the initial bubble radius on bubble radius history for $\theta_w = 10$°C and $\delta_b = 0.06$ mm. The limits for initial bubble radii were taken to be 0.67 and 0.98 mm. These were obtained by adding the measurement uncertainty of ∓ 0.03 mm to the smallest and largest, respectively, radii taken from the second frames of the bubble data. The effect of R_0 seems to cause the curves to run parallel to each other, displaced by a small amount.

It is also important to point out that the solution of equation (17) need not be started from the second movie frame. It one assumes a larger R_0, say 1.5 mm (this represents a location further downstream), the solution of equation (17) would still match the data for the same parameters.

CONCLUSIONS

An analytical and experimental investigation of the ebullition of thin, falling water films has been conducted. A mechanism that models bubble growth has been proposed. This mechanism is believed to be responsible for the large heat transfer rates present in thin falling film boiling. An analysis of the data shows that the bubble base must be deeply imbedded in the thin falling liquid film. In addition, the analysis reveals that a slip velocity appears to exist between the bubble velocity and the velocity of the fluid layer which comprises the bubble base. For the film Reynolds number analyzed, 2070, this slip velocity (770 mm s^{-1}) is quite large, on the same order of magnitude as the bubble velocity (830 mm s^{-1}). A bubble in a falling liquid film must then move faster than the fluid beneath its base. Thus, its leading semicircular base edge is in continuous contact with new superheated liquid. This gives rise to a very large initial thermal gradient through the bubble base at its leading edge. At locations past the leading edge, the thermal gradient at the bubble base becomes smaller because energy is being used up from the liquid layers beneath the bubble base. This energy is transferred into the bubble via liquid evaporation at the bubble base. Hence, the proposed model is valid for cases where the wall heat flux results in negligible mass transfer at the bubble base, i.e. the thickness below the bubble base remains approximately constant.

The growth rate of the falling film bubble differs markedly from that of its pool boiling counterpart, which only moves through superheated fluid at a speed equal to its own radial growth rate. The slip velocities of the falling film bubbles analyzed are an order of magnitude greater than their radial growth velocities. The bubble radial growth histories which result in the falling film case are therefore significantly larger than those of their pool boiling counterpart, for the same film superheat. This was shown by Fig. 9.

In summary, the bubbles in thin falling film ebullition act like local heat extracters that cool the superheated liquid film over which they ride.

REFERENCES

1. Y. Y. Hsu, On the size range of active nucleation cavities on a heating surface, *J. Heat Transfer* **84,** 207–216 (1962).
2. Y. Y. Hsu and R. Graham, *Transport Processes in Boiling and Two Phase Systems*, Chaps. 1, 2. McGraw-Hill, New York (1976).
3. C. Y. Han and P. Griffith, The mechanism of heat transfer in nucleate pool boiling—Part I, *Int. J. Heat Mass Transfer* **8,** 887–904 (1965).
4. T. Fujita and T. Ueda, Heat transfer to falling liquid films and film breakdown—II. Saturated liquid films with nucleate boiling, *Int. J. Heat Mass Transfer* **21,** 109–118 (1978).
5. R. Mesler and G. Mailen, Nucleate boiling in thin liquid films, *A.I.Ch.E. Jl* **23,** 954–957 (1977).
6. W. Parken, Heat transfer to thin water films on horizontal tubes, Ph.D. dissertation, Rutgers University, New Brunswick, New Jersey (1975).
7. M. Cerza and V. Sernas, Nucleate boiling heat transfer in developing laminar falling water films, *Proc. ASME–JSME Joint Thermal Engineering Conference*, Vol. 1, pp. 111–118 (1983).
8. M. Cerza, An investigation into the mechanism for nucleate boiling in thin falling water films, Ph.D. dissertation, Rutgers University, New Brunswick, New Jersey (1983).
9. M. S. Plesset and S. A. Zwick, The growth of vapor bubbles in superheated liquids, *J. appl. Phys.* **25,** 493–500 (1954).
10. H. K. Forster and N. Zuber, Growth of a vapor bubble in a superheated liquid, *J. appl. Phys.* **25,** 473–478 (1954).
11. V. Sernas and F. C. Hooper, The initial vapor bubble growth on a heated wall during nucleate boiling, *Int. J. Heat Mass Transfer* **12,** 1627–1637 (1969).
12. L. E. Scriven, On the dynamics of phase growth, *Chem. Engng Sci.* **10,** 1–12 (1959).
13. V. Sernas and K. Stanzione, Some aspects of the heat transfer mechanism during boiling of falling water films, AIAA paper 81-1064, 16th Thermophysics Conference (1981).
14. L. Graetz, Uber die Warmeleitungsfahigkeit von Flussigkeiten, *Annln Phys. Chem.* **25,** 337–357 (1885).
15. R. Siegel, E. M. Sparrow and T. M. Hallman, Steady

laminar heat transfer with prescribed wall heat flux, *Appl. Sci. Res.* **A7**, 386–391 (1958).
16. R. D. Cess and E. C. Shaffer, Heat transfer to laminar flow between parallel plates with a prescribed wall heat flux, *Appl. Sci. Res.* **A8**, 339–344 (1959).
17. J. R. Sellars, M. Tribus and J. S. Klein, Heat transfer to laminar flow in a round tube or flat conduit—the Graetz problem extended, *Trans. Am. Soc. mech. Engrs* **78**, 441–448 (1956).
18. R. Mesler, A mechanism supported by extensive experimental evidence to explain high heat fluxes observed during nucleate boiling, *A.I.Ch.E. Jl* **22**, 246–252 (1976).

MODELE DE CROISSANCE DE BULLE POUR L'EBULLITION NUCLEE DANS DES FILMS D'EAU MINCES, LAMINAIRES, SURCHAUFFES ET TOMBANTS

Résumé—Une étude analytique et expérimentale est présentée sur la croissance de bulle dans un film d'eau mince, laminaire, surchauffé et tombant. La majorité de la croissance de bulle est causée par la conduction thermique variable à travers la base de la bulle tandis que la bulle est balayée par le film tombant. Les flux thermiques observés sont significativement plus grands que ceux pour l'évaporation à la surface du film. Ceci montre que la base de la bulle est noyée dans l'épaisseur du film. Le modèle proposé est applicable aux cas où le flux thermique pariétal résulte d'un transfert massique négligeable à la base de la bulle.

EIN BLASENWACHSTUMSMODELL FÜR DAS BLASENSIEDEN IN DÜNNEN, FALLENDEN, ÜBERHITZTEN UND LAMINAREN WASSERFILMEN

Zusammenfassung—Es wurden analytische und experimentelle Untersuchungen zum Mechanismus des Blasenwachstums in einem dünnen, fallenden, überhitzten und laminaren Wasserfilm durchgeführt. Es zeigt sich, daß das Blasenwachstum hauptsächlich durch instationäre Wärmeleitung durch den Blasenfuß verursacht wird, während die Blase durch den fallenden Film weggeschwemmt wird. Bei der Blasenbildung sind die beobachteten Wärmeströme deutlich größer als bei reiner Oberflächenverdampfung. Dieses deutet darauf hin, daß der Blasenfuß im umgebenden Film eingebettet ist. Das vorgeschlagene Modell läßt sich für die Fälle anwenden, bei denen die Wärmestromdichte an der Wand einen vernachlässigbaren Massentransport im Blasenfuß zur Folge hat.

МОДЕЛЬ РОСТА ПУЗЫРЬКА ДЛЯ ПУЗЫРЬКОВОГО КИПЕНИЯ В ТОНКИХ СТЕКАЮЩИХ ПЕРЕГРЕТЫХ ЛАМИНАРНЫХ ПЛЕНКАХ ВОДЫ

Аннотация—Проведено аналитическое и экспериментальное исследование механизма роста пузырька в тонкой стекающей перегретой ламинарной пленке воды. Найдено, что в основном рост пузырьков вызывается теплопроводностью в месте присоединения пузырька во время уноса пузырька стекающей пленкой. Наблюдаемые скорости роста пузырька за счет теплопроводности значительно выше тех, которые возникают только при испарении поверхностной пленки. Это указывает на то, что место присоединения пузырька погружено в толщу окружающей пленки. Предложенная модель применима к случаям, когда тепловые потоки на поверхности приводят к пренебрежимо малому переносу массы основания пузырька.